

Interaction-driven topological phase transitions in fermionic SU(3) systems

Mohsen Hafez-Torbati,^{1,*} Jun-Hui Zheng,^{1,2} Bernhard Irsigler,¹ and Walter Hofstetter^{1,†}

¹*Institut für Theoretische Physik, Goethe-Universität, 60438 Frankfurt/Main, Germany.*

²*Center for Quantum Spintronics, Department of Physics,*

Norwegian University of Science and Technology, NO-7491 Trondheim, Norway

(Dated: June 26, 2020)

We consider SU(3) fermions on the triangular lattice in the presence of a gauge potential which stabilizes a quantum Hall insulator (QHI) at the density of one particle per lattice site. We investigate the effect of the Hubbard interaction, favoring magnetic long-range order, and a three-sublattice potential (TSP), favoring a normal insulator (NI), on the system. For weak TSP we find that the Hubbard interaction drives the QHI into a three-sublattice magnetic Mott insulator (MMI). For intermediate values of TSP we identify two transition points upon increasing the Hubbard interaction. The first transition is from the NI to the QHI and the second transition is from the QHI to the MMI. For large values of the TSP a charge-ordered magnetic insulator (COMI) emerges between the NI and the QHI, leading to an interaction-driven COMI-to-QHI transition.

I. INTRODUCTION

Since the experimental discovery of the quantum Hall effect in two-dimensional (2D) electron systems¹ novel types of band insulators such as quantum Hall (QHI)² and quantum spin Hall (QSHI) insulator³ have been identified, which are characterized by topological invariants and can not be adiabatically connected to the previously-known normal insulators (NIs)⁴. The QHI occurs at particular particle fillings when a constant magnetic field is applied perpendicular to a 2D lattice potential, splitting a single energy band into several subbands⁵, each one carrying an integer quantum number² called Chern number⁶. The QSHI is a result of time-reversal symmetry and spin-orbit coupling and is characterized by a \mathbb{Z}_2 topological invariant⁷.

The effect of interaction on a band insulator (BI) and emergence of Mott physics in the strong coupling regime has been an interesting problem for a long time⁸, initially motivated by the observation of neutral-ionic phase transition in organic compounds⁹. A spontaneously dimerized phase^{10–13} stabilized by condensation of a singlet exciton^{14–17} separates the NI from Mott insulator (MI) as is studied via the 1D ionic Hubbard model. The ground state phase diagram of the 2D model is controversial^{18–20}.

In recent years, there has been a large interest in interacting topological insulators²¹, with a focus on realizing topological many-body quantum states such as fractional QHI²² and studying interaction-driven topological phase transitions^{23–28}. In the time-reversal-invariant Harper-Hofstadter-Hubbard model with a spin-mixing hopping term an interaction-driven NI-to-QSHI transition is identified²³, which is found also in an extended Bernevig-Hughes-Zhang-Hubbard model^{24,25}. The competition of the Hubbard interaction and the staggered potential in the Haldane-Hubbard model stabilizes an antiferromagnetic Chern insulator (AFCI) where one of the spin components is in the quantum Hall and the other in the normal state^{26,27}. Such an AFCI is proposed also for the Kane-Mele-Hubbard model but with a spontaneous

breaking of the time-reversal symmetry²⁸.

Spin-orbit coupling in multicomponent systems can give rise to a richer topological band structure compared to the SU(2) case^{29–31}. In the Mott regime SU(N) systems are potential candidates to find novel ordered and disordered MIs^{32–37}. Furthermore, interaction-driven metallic phases and a charge-ordered magnetic insulator (COMI) are reported as a result of competing charge and magnetic order in fermionic SU(3) systems³⁸.

Here we investigate SU(3) fermions on the triangular lattice at $1/3$ filling in the presence of a gauge potential stabilizing a QHI. We study the effect of the Hubbard interaction and a three-sublattice potential (TSP) on the QHI phase. For weak TSP, the Hubbard interaction drives the QHI into a three-sublattice magnetic MI (MMI). For intermediate values of the TSP we find the NI at weak and the MMI at strong Hubbard U , separated by a QHI. For large TSP an additional COMI phase emerges between the NI and the QHI. This leads to the realization of an interaction-driven COMI-to-QHI transition. The study is experimentally motivated by the recent progress in realization of artificial gauge fields^{39–42} and creation of SU(N)-symmetric multicomponent systems^{43–47} in optical lattices. The Hamiltonian reads

$$H = -t \sum_{\langle \mathbf{r}\mathbf{r}' \rangle} \sum_{\alpha} \left(e^{2\pi i \phi_{\mathbf{r},\mathbf{r}'}} c_{\mathbf{r}'\alpha}^{\dagger} c_{\mathbf{r}\alpha} + \text{H.c.} \right) + \sum_{\mathbf{r}\alpha} \Delta_{\mathbf{r}} n_{\mathbf{r}\alpha} + U \sum_{\mathbf{r}} \sum_{\alpha < \alpha'} n_{\mathbf{r}\alpha} n_{\mathbf{r}\alpha'} \quad , \quad (1)$$

where $c_{\mathbf{r}\alpha}^{\dagger}$ is the fermionic creation operator at the lattice position \mathbf{r} with the spin component α , $n_{\mathbf{r}\alpha} = c_{\mathbf{r}\alpha}^{\dagger} c_{\mathbf{r}\alpha}$ is the occupation number operator, and the summation over $\langle \mathbf{r}\mathbf{r}' \rangle$ restricts the hopping to nearest-neighbor sites. The hopping phase factors $\phi_{\mathbf{r},\mathbf{r}'}$ around each triangle add up to a constant Φ which describes the magnetic flux going through each triangle in units of the magnetic flux quantum. The three sublattices A , B , and C of the tripartite triangular lattice acquire respectively the onsite energies $-\Delta_1$, 0 , and $+\Delta_2$ due to the second term, the TSP. The last term is the Hubbard interaction.

II. TECHNICAL ASPECTS

We map the triangular lattice to the square lattice with hopping along the \hat{x} , \hat{y} , and $(\hat{x} + \hat{y})$ directions. We consider the hopping phase factors $\phi_{\mathbf{r},\mathbf{r}+\hat{x}} = 0$, $\phi_{\mathbf{r},\mathbf{r}+\hat{y}} = (2m+2n+1)\Phi$, and $\phi_{\mathbf{r},\mathbf{r}+\hat{x}+\hat{y}} = 2(m+n+1)\Phi$ from the lattice position $\mathbf{r} = m\hat{x} + n\hat{y}$, where a is the lattice constant and $m, n \in \mathbb{Z}$ ⁴⁸. There are three sites in the unit cell for $\Phi = 1/6$, which is the flux we consider in this paper. In the absence of interaction the Hamiltonian reduces to a three-level problem in momentum space leading to three distinct Bloch bands with a three-fold spin degeneracy each. We determine the Chern number of the system at $U = 0$ using twisted boundary conditions^{49,50}. We employ real-space dynamical mean-field theory (DMFT)^{51–53} which we implemented for $SU(N)$ systems in Ref. 36 to address the Hamiltonian at finite U . In real-space DMFT the self-energy is approximated to be local but it can be position-dependent. We consider $L \times L$ lattices with $L = 30$ and periodic boundary conditions unless mentioned otherwise. We use the exact diagonalization (ED) impurity solver with four and five bath sites and check that the results nicely agree across different transition points. The presented results are for five bath sites unless mentioned otherwise. We have used the inverse temperature $\beta = 32/t$. We find at different selected parameter values that the results remain unchanged compared to the ones obtained using a zero temperature ED impurity solver⁵⁴. We expect that a temperature $T = t/32$ is low enough to capture the ground state properties of the model.

We evaluate the Chern number of the interacting system using the topological Hamiltonian approach⁵⁵. This method states that the Chern number of an interacting system is equal to the Chern number of an effective non-interacting model called “topological Hamiltonian”, which in the Bloch form reads

$$h_t(\mathbf{k}) = h_0(\mathbf{k}) + \Sigma(\mathbf{k}, i\omega = 0), \quad (2)$$

where $h_0(\mathbf{k})$ is the non-interacting part of the original model and $\Sigma(\mathbf{k}, i\omega)$ stands for the self-energy. In DMFT the self-energy is local and we have no element in the Hamiltonian and in the self-energy linking different spin components. Consequently, the effect of self-energy in Eq. (2) will be to renormalize the TSP to

$$\tilde{\Delta}_{1,\alpha} = \Delta_1 + \left(\Sigma_{B,\alpha}(0) - \Sigma_{A,\alpha}(0) \right), \quad (3a)$$

$$\tilde{\Delta}_{2,\alpha} = \Delta_2 + \left(\Sigma_{C,\alpha}(0) - \Sigma_{B,\alpha}(0) \right), \quad (3b)$$

up to an irrelevant shift in the energy spectrum. We have used $\Sigma_{A,\alpha}(0)$ for the zero-frequency self-energy on sublattice A with spin component α and similarly for sublattices B and C ⁵⁶. The effective TSP Eq. (3) in paramagnetic phases is spin-independent, while in magnetically ordered phases, i.e., in phases with broken $SU(3)$ symmetry, it depends on the spin. This shows that different spin components can in principle occur in distinct topological regions.

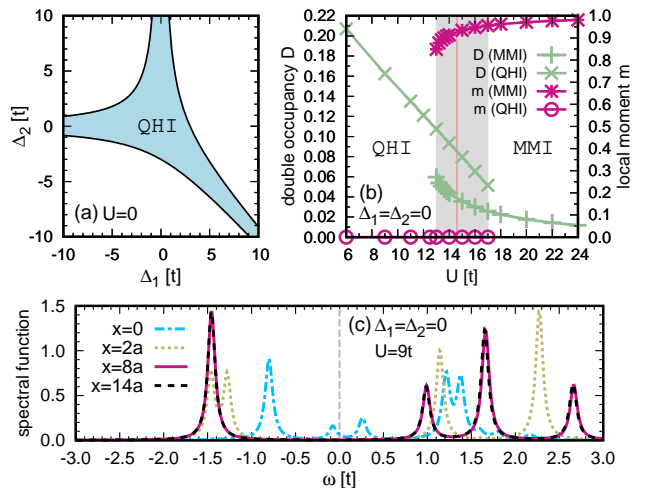


Figure 1. (a) Phase diagram of the model for the Hubbard interaction $U = 0$ in the Δ_1 - Δ_2 plane. The shaded area corresponds to the quantum Hall insulator (QHI) and the white area to the normal insulator (NI). (b) The double occupancy and the local moment in the QHI and in the magnetic Mott insulator (MMI) versus U at $\Delta_1 = \Delta_2 = 0$. The gray area is the coexistence region and the vertical solid line marks the transition point. (c) The spectral function $A_{r\alpha}(\omega)$ at $U = 9t$ and $\Delta_1 = \Delta_2 = 0$ versus frequency ω for a cylindrical geometry with edges at $x = 0$ and $x = 29a$.

III. RESULTS

Fig. 1(a) shows the phase diagram of the model at $U = 0$ in the Δ_1 - Δ_2 plane. The shaded area denotes the QHI and the white area the NI phase. In the QHI each spin component α contributes a Chern number $\mathcal{C}_\alpha = 1$, leading to the Chern number $\mathcal{C} = 3$ for the full system. The three asymptotic branches for the phase boundaries can be understood based on the sublattice degeneracy. For instance, sublattices A and B are degenerate at $\Delta_1 = 0$ and upon increasing $\Delta_2 \rightarrow +\infty$ always the two lowest Bloch bands remain topological, leading to a QHI state at 1/3 filling. Fig. 1(a) can be used to determine also the topological properties of the interacting model as the effect of the interaction is only to renormalize the TSP.

For $SU(3)$ systems we define the double occupancy $D_{\mathbf{r}} = \sum_{\alpha < \alpha'} \langle n_{\mathbf{r}\alpha} n_{\mathbf{r}\alpha'} \rangle$ and the local moment $m_{\mathbf{r}} = \sqrt{3} |\langle \mathcal{S}_{\mathbf{r}} \rangle| / 2$ where $\mathcal{S}_{\mathbf{r}}^i = \sum_{\alpha\alpha'} c_{\mathbf{r}\alpha}^\dagger \lambda_{\alpha\alpha'}^i c_{\mathbf{r}\alpha'}$ for $i = 1, \dots, 8$ define the elements of the eight-dimensional pseudospin operator $\mathcal{S}_{\mathbf{r}}$ with λ^i being the Gell-Mann matrices. In magnetic phases there is a continuous degeneracy and we focus on the solution with pseudospin order in the \hat{S}_3 - \hat{S}_8 plane. In Fig. 1(b) the double occupancy and the local moment in the QHI and in the MMI are depicted versus U for $\Delta_1 = \Delta_2 = 0$. The QHI and the MMI are two DMFT solutions coexisting in the gray area. The QHI results from the zero effective TSP in the paramagnetic region. The MMI is topologically trivial as we find all the three spin components in the normal state. This is a point which we will discuss further in Fig. 3. For

$\Delta_1 = \Delta_2 = 0$ D_r and m_r are position-independent. The red solid line at $U_c \simeq 14.5t$ specifies the transition point obtained by comparing the energy of the two states. The MMI has a three-sublattice magnetic order such that on each sublattice one of the spin components has the dominant density and the density of the other two components is equal, leading to a 120° pseudospin order^{36,57}.

To investigate gapless edge states in the QHI we consider a 30×30 lattice with periodic boundary condition along \hat{y} and open boundary condition along \hat{x} , i.e., a cylindrical geometry, with edges at $x = 0$ and $x = 29a$. The spectral function at position \mathbf{r} for the spin component α is defined from the local Green's function as $A_{\mathbf{r}\alpha}(\omega) = -\frac{1}{\pi} \text{Im} G_{\mathbf{r}\alpha}(\omega + i\epsilon)$ where ϵ is a numerical broadening factor. In Fig. 1(c) the spectral function $A_{\mathbf{r}\alpha}(\omega)$ for $U = 9t$ and $\Delta_1 = \Delta_2 = 0$ is plotted versus frequency ω in the range $-3t < \omega < 3t$ with $\epsilon = 0.05t$. The dashed line at $\omega = 0$ specifies the Fermi energy. Due to the finite number of bath sites $N_b = 5$ in the impurity problem the fine details of the spectral function can not be reserved. However, one can clearly identify the spectral contribution from the edge $x = 0$ near the Fermi energy, which vanishes upon approaching the bulk $x = 14a$. It is interesting that even with a finite number of bath sites one can see evidence of gapless edge states. The edge and the bulk spectral function on finite clusters in an interacting topological insulator is discussed also in Ref.⁵⁸. However, we notice that computing topological invariants is a more accurate and reliable way to recognize topological phase transitions.

We leave a general study of the Hubbard interaction on the phase diagram Fig. 1(a) for future research and consider here for simplicity $\Delta_1 = \Delta_2 =: \Delta > 0$. We believe that small deviations from this symmetric case will not change the physics discussed in the following essentially. At $U = 0$ there is a transition from the QHI to the NI at $\Delta_c = 3t/\sqrt{2}$ upon increasing Δ . In Fig. 2 we have plotted the double occupancy D_A and the local moment m_A on sublattice A as well as the Chern number C_α versus the Hubbard interaction U for $\Delta = 6t$ (a) and $\Delta = 11t$ (b). To avoid a busy figure the local moment is given only in magnetic phases (MP) as it is trivially zero in paramagnetic phases (PP). In addition we find $C_\alpha = 0$ for all the three spin components in MP, see also below. The given spin-independent C_α is for PP. The gray area indicates coexistence of magnetic and paramagnetic DMFT solutions. One notices that in Fig. 2(b) the COMI always coexists with a paramagnetic phase and the given Chern number is for the paramagnetic phase not for the COMI. The red vertical solid line specifies the transition point and is obtained by comparing the energies of the two states in the case of coexistence. The blue vertical dashed line denotes the NI-to-QHI transition in the case that paramagnetic solution is enforced.

One can see from Fig. 2(a) that the Hubbard interaction drives the NI into the QHI and subsequently the QHI into the MMI. Similar sequences of phase transitions are found in SU(2) topological systems^{23–28}. Upon

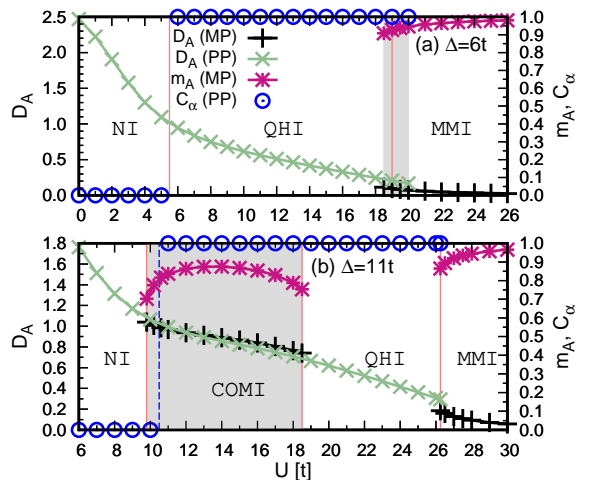


Figure 2. The double occupancy D_A and the local moment m_A on sublattice A , and the Chern number C_α for the spin component α versus the Hubbard interaction U for $\Delta = 6t$ (a) and $\Delta = 11t$ (b). The gray area denotes coexistence of magnetic and paramagnetic solutions. The local moment m_A is given only in magnetic phases (MP), i.e., in the charge-ordered magnetic insulator (COMI) and in the magnetic Mott insulator (MMI). The given spin-independent Chern number C_α is for paramagnetic phases (PP), i.e., for the normal insulator (NI) and for the quantum Hall insulator (QHI), as it is zero for MP. The red solid lines mark the transition points and the dashed blue line denotes the NI-to-QHI transition ignoring the magnetic DMFT solution.

increasing the TSP to $\Delta = 11t$ in Fig. 2(b) a COMI phase emerges between the NI and the QHI. In the COMI phase, sublattice A is almost doubly occupied with two spin components, sublattice B is mainly occupied with the third component, and sublattice C is almost empty. The local moment on sublattice A and B is equal and it is zero on sublattice C . There is a 180° pseudospin order on sublattices A and B ³⁸. We find that the COMI always has a lower energy than the paramagnetic phases, i.e., the NI and the QHI are metastable. We notice that charge order is an intrinsic property of the COMI phase as it is not adiabatically connected to any phase with a uniform charge distribution. This is to be compared with the QHI and MMI phases which are adiabatically connected to $\Delta = 0$ limit where the charge distribution is uniform. We believe the Hubbard interaction driving a magnetic phase into a quantum Hall state as it occurs in the COMI-to-QHI transition is a peculiar feature of multicomponent systems which has no SU(2) counterpart.

The double occupancy D_A versus U in Fig. 2 exhibits a change of slope in different phases and can be conveniently measured in optical lattices using the photoassociation technique⁴⁶. The magnetic order can be identified using a quantum gas microscope^{59,60}. Lower temperatures are accessible in multicomponent systems compared to the SU(2) case due to a Pomeranchuk cooling effect⁶¹. We notice that to realize magnetic order at finite temperature in our system a weak coupling in the

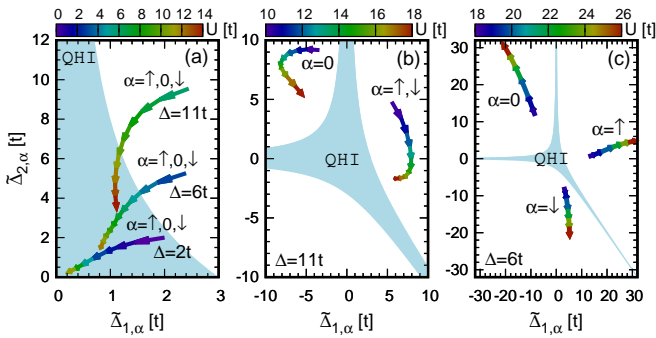


Figure 3. The evolution of the effective potential as a function of U for the paramagnetic DMFT solution (a) for the charge-ordered magnetic insulator with $\Delta = 11t$ (b) and for the magnetic Mott insulator with $\Delta = 6t$ (c) for the spin components $\alpha = \uparrow, 0$, and \downarrow .

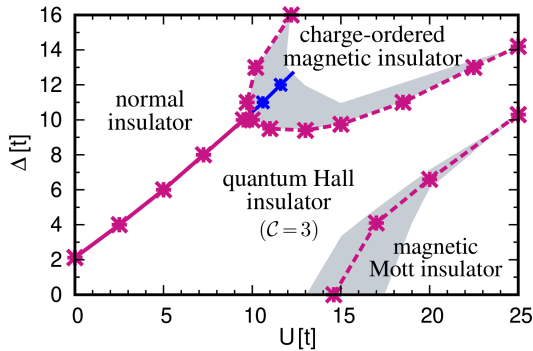


Figure 4. The phase diagram in the U - Δ plane. The red lines denote the phase boundaries, the gray areas represent the coexistence regions, and the blue line separates the normal from the quantum Hall insulator when ignoring the magnetic DMFT solution. The solid (dashed) line indicates a continuous (discontinuous) transition.

third direction or an interaction anisotropy is required.

To further clarify the topological nature of different phases we study in Fig. 3 the evolution of the effective TSP as a function of U for the paramagnetic DMFT solution (a), for the COMI with $\Delta = 11t$ (b), and for the MMI with $\Delta = 6t$ (c). The direction of the curves are upon increasing U . The shaded area corresponds to QHI and the white area to NI. One sees from Fig. 3(a) that for $\Delta = 2t$ the system is always in the QHI region but for $\Delta = 6t$ and $\Delta = 11t$ a NI-to-QHI transition occurs. Figs. 3(b) and 3(c) demonstrate that the COMI and the MMI are topologically trivial as all the three spin components $\alpha = \uparrow, 0$, and \downarrow are in the NI region. The larger the local moment is in the MMI and in the COMI in Figs. 2(a) and 2(b) the deeper the corresponding topological Hamiltonian is in the NI in Fig. 3. The interaction-driven topological phase transitions can be studied in optical lattices using the tomography scheme proposed in Ref. 62.

Fig. 4 displays the phase diagram in the U - Δ plane. The gray areas denote the coexistence of magnetic and

paramagnetic states, the red lines are the phase boundaries, and the blue line separates the NI from the QHI ignoring the magnetic DMFT solution. The solid (dashed) line indicates a continuous (discontinuous) transition. We have used four bath sites in the impurity problem due to the large number of data we needed to produce. However, by comparing Fig. 4 with Fig. 1(b) and Fig. 2 one can see the nice agreement for coexistence regions and transition points obtained with five and four bath sites. We have performed further checks across some other selective transition points. We always find that the NI-to-QHI transition is continuous, although discontinuous transitions in two-orbital systems are also reported²⁵. The coexistence regions shrink upon increasing Δ . The QHI in the limit $U, \Delta \gg t$ appears around $U = 2\Delta$ where the COMI and the MMI are degenerate in the atomic limit, i.e., at $t = 0$ ³⁸. We have produced the phase diagram up to $U = 32t$ and $\Delta = 20t$ and the QHI persists with a constant width. This width is proportional to t and vanishes in the atomic limit.

IV. SUMMARY AND OUTLOOK

To summarize, in recent years there has been a large interest in fermionic $SU(N)$ systems^{32,47} as well as in artificial gauge fields^{63–65} due to their possible realization in optical lattices. While studies of $SU(N)$ systems have mainly been focused on topological states in the absence of interaction^{29–31} and on Mott states in the strong coupling limit^{32–37}, less attention has so far been paid to the competition of band and Mott insulator and possible emergence of intermediate phases and novel phenomena. This requires tuning the interaction from weak to strong which can experimentally be achieved by Feshbach resonances^{66–68}. In this paper we show that local correlations, which are best known for the famous Mott transition, can drive a magnetic phase into a quantum Hall state in multicomponent systems. \mathbb{Z}_2 lattice gauge theories are recently simulated using ultracold atoms in optical lattices^{69,70}. Our work sets the stage for a generalization of static gauge fields with interactions to the dynamical case and for studies of \mathbb{Z}_3 lattice gauge theories, which are linked to important issues in high-energy physics.

V. ACKNOWLEDGEMENT

We would like to thank J. Panas for useful discussions. This work was supported by the Deutsche Forschungsgemeinschaft (DFG, German Research Foundation) under Project No. 277974659 via Research Unit FOR 2414. This work was also supported by the DFG via the high performance computing center LOEWE-CSC.

- * torbati@itp.uni-frankfurt.de
† hofstett@physik.uni-frankfurt.de
- ¹ K. v. Klitzing, G. Dorda, and M. Pepper, *Phys. Rev. Lett.* **45**, 494497 (1980).
 - ² D. J. Thouless, M. Kohmoto, M. P. Nightingale, and M. den Nijs, *Phys. Rev. Lett.* **49**, 405408 (1982).
 - ³ C. L. Kane and E. J. Mele, *Phys. Rev. Lett.* **95**, 226801 (2005).
 - ⁴ M. Z. Hasan and C. L. Kane, *Rev. Mod. Phys.* **82**, 30453067 (2010).
 - ⁵ D. R. Hofstadter, *Phys. Rev. B* **14**, 22392249 (1976).
 - ⁶ B. Simon, *Phys. Rev. Lett.* **51**, 21672170 (1983).
 - ⁷ C. L. Kane and E. J. Mele, *Phys. Rev. Lett.* **95**, 146802 (2005).
 - ⁸ N. Nagaosa and J. Takimoto, *Journal of the Physical Society of Japan* **55**, 27352744 (1986).
 - ⁹ J. B. Torrance, J. E. Vazquez, J. J. Mayerle, and V. Y. Lee, *Phys. Rev. Lett.* **46**, 253257 (1981).
 - ¹⁰ M. Fabrizio, A. O. Gogolin, and A. A. Nersisyan, *Phys. Rev. Lett.* **83**, 20142017 (1999).
 - ¹¹ S. R. Manmana, V. Meden, R. M. Noack, and K. Schnhammer, *Phys. Rev. B* **70**, 155115 (2004).
 - ¹² C. D. Batista and A. A. Aligia, *Phys. Rev. Lett.* **92**, 246405 (2004).
 - ¹³ K. Loida, J.-S. Bernier, R. Citro, E. Orignac, and C. Kolath, *Phys. Rev. Lett.* **119**, 230403 (2017).
 - ¹⁴ M. Hafez Torbati, N. A. Drescher, and G. S. Uhrig, *Phys. Rev. B* **89**, 245126 (2014).
 - ¹⁵ M. Hafez-Torbati, N. A. Drescher, and G. S. Uhrig, *The European Physical Journal B* **88**, 3 (2015).
 - ¹⁶ M. Hafez and S. A. Jafari, *The European Physical Journal B* **78**, 323333 (2010).
 - ¹⁷ M. Hafez and M. Abolhassani, *Journal of Physics: Condensed Matter* **23**, 245602 (2011).
 - ¹⁸ N. Paris, K. Bouadim, F. Hbert, G. G. Batrouni, and R. T. Scalettar, *Phys. Rev. Lett.* **98**, 046403 (2007).
 - ¹⁹ S. S. Kancharla and E. Dagotto, *Phys. Rev. Lett.* **98**, 016402 (2007).
 - ²⁰ M. Hafez-Torbati and G. S. Uhrig, *Phys. Rev. B* **93**, 195128 (2016).
 - ²¹ S. Rachel, *Reports on Progress in Physics* **81**, 116501 (2018).
 - ²² S. A. Parameswaran, R. Roy, and S. L. Sondhi, *Comptes Rendus Physique* **14**, 816 (2013), topological insulators / Isolants topologiques.
 - ²³ D. Cocks, P. P. Orth, S. Rachel, M. Buchhold, K. Le Hur, and W. Hofstetter, *Phys. Rev. Lett.* **109**, 205303 (2012).
 - ²⁴ J. C. Budich, B. Trauzettel, and G. Sangiovanni, *Phys. Rev. B* **87**, 235104 (2013).
 - ²⁵ A. Amaricci, J. C. Budich, M. Capone, B. Trauzettel, and G. Sangiovanni, *Phys. Rev. Lett.* **114**, 185701 (2015).
 - ²⁶ J. He, Y.-H. Zong, S.-P. Kou, Y. Liang, and S. Feng, *Phys. Rev. B* **84**, 035127 (2011).
 - ²⁷ T. I. Vanhala, T. Siro, L. Liang, M. Troyer, A. Harju, and P. Trm, *Phys. Rev. Lett.* **116**, 225305 (2016).
 - ²⁸ K. Jiang, S. Zhou, X. Dai, and Z. Wang, *Phys. Rev. Lett.* **120**, 157205 (2018).
 - ²⁹ R. Barnett, G. R. Boyd, and V. Galitski, *Phys. Rev. Lett.* **109**, 235308 (2012).
 - ³⁰ U. Bornheimer, C. Miniatura, and B. Grmaud, *Phys. Rev. A* **98**, 043614 (2018).
 - ³¹ M. H. Yau and C. A. R. S. de Melo, arXiv e-prints, arXiv:1904.12791 (2019), [arXiv:1904.12791](https://arxiv.org/abs/1904.12791) [cond-mat.quant-gas].
 - ³² A. V. Gorshkov, M. Hermele, V. Gurarie, C. Xu, P. S. Julienne, J. Ye, P. Zoller, E. Demler, M. D. Lukin, and A. M. Rey, *Nature Physics* **6**, 289295 (2010).
 - ³³ T. A. Tóth, A. M. Läuchli, F. Mila, and K. Penc, *Phys. Rev. Lett.* **105**, 265301 (2010).
 - ³⁴ Z. Zhou, D. Wang, Z. Y. Meng, Y. Wang, and C. Wu, *Phys. Rev. B* **93**, 245157 (2016).
 - ³⁵ P. Nataf, M. Lajk, A. Wietek, K. Penc, F. Mila, and A. M. Luchli, *Phys. Rev. Lett.* **117**, 167202 (2016).
 - ³⁶ M. Hafez-Torbati and W. Hofstetter, *Phys. Rev. B* **98**, 245131 (2018).
 - ³⁷ S. S. Chung and P. Corboz, *Phys. Rev. B* **100**, 035134 (2019).
 - ³⁸ M. Hafez-Torbati and W. Hofstetter, *Phys. Rev. B* **100**, 035133 (2019).
 - ³⁹ M. Aidelsburger, M. Atala, M. Lohse, J. T. Barreiro, B. Paredes, and I. Bloch, *Phys. Rev. Lett.* **111**, 185301 (2013).
 - ⁴⁰ H. Miyake, G. A. Siviloglou, C. J. Kennedy, W. C. Burton, and W. Ketterle, *Phys. Rev. Lett.* **111**, 185302 (2013).
 - ⁴¹ G. Jotzu, M. Messer, R. Desbuquois, M. Lebrat, T. Uehlinger, D. Greif, and T. Esslinger, *Nature* **515**, 237 (2014).
 - ⁴² M. Aidelsburger, *Journal of Physics B: Atomic, Molecular and Optical Physics* **51**, 193001 (2018).
 - ⁴³ T. B. Ottenstein, T. Lompe, M. Kohonen, A. N. Wenz, and S. Jochim, *Phys. Rev. Lett.* **101**, 203202 (2008).
 - ⁴⁴ J. H. Huckans, J. R. Williams, E. L. Hazlett, R. W. Stites, and K. M. O'Hara, *Phys. Rev. Lett.* **102**, 165302 (2009).
 - ⁴⁵ H. Hara, Y. Takasu, Y. Yamaoka, J. M. Doyle, and Y. Takahashi, *Phys. Rev. Lett.* **106**, 205304 (2011).
 - ⁴⁶ S. Taie, R. Yamazaki, S. Sugawa, and Y. Takahashi, *Nature Physics* **8**, 825830 (2012).
 - ⁴⁷ M. A. Cazalilla and A. M. Rey, *Reports on Progress in Physics* **77**, 124401 (2014).
 - ⁴⁸ These phase factors can be obtained using the Peierls substitution for the gauge field $\mathbf{A} = B(x+y)\hat{y}$ which describes the magnetic field $\mathbf{B} = B\hat{z}$. The advantage of the chosen gauge over the Landau gauge is that it makes the hopping phase factors depend on $(x+y)$, which is the same position dependency as in the three-sublattice potential, and consequently reduces the number of sites in the unit cell.
 - ⁴⁹ Q. Niu, D. J. Thouless, and Y.-S. Wu, *Phys. Rev. B* **31**, 3372 (1985).
 - ⁵⁰ K. Kudo, H. Watanabe, T. Kariyado, and Y. Hatsugai, *Phys. Rev. Lett.* **122**, 146601 (2019).
 - ⁵¹ M. Potthoff and W. Nolting, *Phys. Rev. B* **59**, 2549 (1999).
 - ⁵² Y. Song, R. Wortis, and W. A. Atkinson, *Phys. Rev. B* **77**, 054202 (2008).
 - ⁵³ M. Snoek, I. Titvinidze, C. Tke, K. Byczuk, and W. Hofstetter, *New Journal of Physics* **10**, 093008 (2008).
 - ⁵⁴ M. Caffarel and W. Krauth, *Phys. Rev. Lett.* **72**, 1545 (1994).
 - ⁵⁵ Z. Wang and S.-C. Zhang, *Phys. Rev. X* **2**, 031008 (2012).
 - ⁵⁶ We find that the real-part of the self-energy at the smallest (in absolute value) Matsubara frequency accurately describes the zero-frequency self-energy obtained by a polynomial fit.

- ⁵⁷ B. Bauer, P. Corboz, A. M. Luchli, L. Messio, K. Penc, M. Troyer, and F. Mila, *Phys. Rev. B* **85**, 125116 (2012).
- ⁵⁸ C. N. Varney, K. Sun, M. Rigol, and V. Galitski, *Phys. Rev. B* **82**, 115125 (2010).
- ⁵⁹ A. Mazurenko, C. S. Chiu, G. Ji, M. F. Parsons, M. Karsznagy, R. Schmidt, F. Grusdt, E. Demler, D. Greif, and M. Greiner, *Nature* **545**, 462 (2017).
- ⁶⁰ P. T. Brown, D. Mitra, E. Guardado-Sanchez, P. Schau, S. S. Kondov, E. Khatami, T. Paiva, N. Trivedi, D. A. Huse, and W. S. Bakr, *Science* **357**, 13851388 (2017).
- ⁶¹ H. Ozawa, S. Taie, Y. Takasu, and Y. Takahashi, *Phys. Rev. Lett.* **121**, 225303 (2018).
- ⁶² Zheng Jun-Hui, Irsigler Bernhard, Jiang Lijia, Weitenberg Christof, and Hofstetter Walter, *Phys. Rev. A* **101**, 013631 (2020).
- ⁶³ M. Aidelsburger, S. Nascimbene, and N. Goldman, *Comptes Rendus Physique* **19**, 394432 (2018), quantum simulation / Simulation quantique.
- ⁶⁴ N. R. Cooper, J. Dalibard, and I. B. Spielman, *Rev. Mod. Phys.* **91**, 015005 (2019).
- ⁶⁵ W. Hofstetter and T. Qin, *Journal of Physics B: Atomic, Molecular and Optical Physics* **51**, 082001 (2018).
- ⁶⁶ S. Inouye, M. R. Andrews, J. Stenger, H.-J. Miesner, D. M. Stamper-Kurn, and W. Ketterle, *Nature* **392**, 151154 (1998).
- ⁶⁷ P. Courteille, R. S. Freeland, D. J. Heinzen, F. A. van Abeelen, and B. J. Verhaar, *Phys. Rev. Lett.* **81**, 6972 (1998).
- ⁶⁸ I. Bloch, J. Dalibard, and W. Zwerger, *Rev. Mod. Phys.* **80**, 885 (2008).
- ⁶⁹ L. Barbiero, C. Schweizer, M. Aidelsburger, E. Demler, N. Goldman, and F. Grusdt, *Science Advances* **5**, eaav7444 (2019).
- ⁷⁰ Schweizer Christian, Grusdt Fabian, Berngruber Moritz, Barbiero Luca, Demler Eugene, Goldman Nathan, Bloch Immanuel, and Aidelsburger Monika, *Nature Physics* **15**, 1168 (2019).